Applied Surface Science 256 (2010) 2532–2538

Contents lists available at ScienceDirect

Applied Surface Science

journal homepage: www.elsevier.com/locate/apsusc

Oriented single crystalline TiO_2 nano-pillar arrays directly grown on titanium substrate in tetramethylammonium hydroxide solution

Xiang Dong, Jie Tao *, Yingying Li, Hong Zhu

College of Material Science and Technology, Nanjing University of Aeronautics and Astronautics, Nanjing 210016, PR China

ARTICLE INFO

Article history:
Received 3 September 2009
Received in revised form 13 October 2009
Accepted 29 October 2009
Available online 6 November 2009

Keywords:
TiO_2
Nano-pillar arrays
One-step synthesis
Hydrothermal

ABSTRACT

Oriented single crystalline titanium dioxide (TiO_2) nano-pillar arrays were directly synthesized on the Ti plate in tetramethylammonium hydroxide (TMAOH) solution by one-pot hydrothermal method. The samples were characterized respectively by means of field-emission scanning electron microscopy (FESEM), transmission electron microscopy (TEM), high-resolution transmission electron microscopy (HRTEM), and X-ray diffraction (XRD). Results showed that the TiO_2 nano-pillar with a tetrahydral bipyramidal tip grew vertically on the titanium substrate. HRTEM and Raman results confirmed that the TiO_2 nano-pillar arrays were single crystalline anatase. The controls of morphology, size, and orientation of the nano-pillar could be achieved by varying the solution concentration and hydrothermal temperature. Furthermore, the special morphology of the TiO_2 nano-pillar arrays was caused by the selectively absorption of the tetramethylammonium (TMA) through hydrogen bonds on the lattice planes parallel to (0 0 1) of anatase TiO_2. Less grain boundaries and direct electrical pathway for electron transferring were crucial for the superior photoelectrochemical properties of the single anatase TiO_2 nano-pillar arrays. This approach provides a facile in situ method to synthesize TiO_2 nano-pillar arrays with a special morphology on titanium substrate.

© 2009 Elsevier B.V. All rights reserved.

1. Introduction

Owing to the excellent chemical and photochemical stability, high surface and interfacial areas, ideal photoelectrochemical properties, and directional electron transport ability, one-dimensional nanostructure titania (TiO_2) including nanorods, nanowires, nano-pillars and nanotubes are promising materials for numerous applications, such as water photoelectrolysis [1], gas sensors [2], dye-sensitized or Gratzel solar cell (DSSC) [3], and photonic materials [4,5]. Especially for solar cells, the single crystal TiO_2 with array architectures can provide direct electrical pathway for photogenerated electrons and enhance the electron transport rate. Therefore, the performance of the photocatalytic and photovoltaic devices (such as DSSC) would be improved [6]. Indeed, a very remarkable result of DSSC based on TiO_2 nanowire array has been obtained [7].

Recently, more and more attention has been paid on one-dimensional aligned nano-TiO_2 array. Considerable efforts have focused on the synthesis of oriented one-dimensional TiO_2 nanostructures. The synthesizing methods include high temperature oxidation [8], anode oxidation [9], glass phase topotaxy growth (GPT) method [10], templated sol–gel methods [11], electron beam deposition [12], metal organic chemical vapor deposition (MOCVD) [13], etc. However, these methods are complicated, costly, and not suitable for large-scale preparation. Therefore, a one-step template-free synthesizing route for one-dimensional TiO_2 array becomes a significant challenge for researchers.

Nowadays, substrate-anchored thin film and coating of oriented nanostructures are often more desirable for application [14]. Wu et al. [15,16] prepared ordered TiO_2 nanorods by using directly oxidizing a Ti plate with H_2O_2 solution, showing high photocatalytic activity. Tian et al. [17] synthesized TiO_2 nanotube array on Ti foil by hydrothermal method, which is an exciting addition to a fast growing family of oriented one-dimensional nanostructure TiO_2. Hydrothermal method with simple and convenient advantages is frequently used to synthesize well crystallized nano-materials with uniform special morphology [18]. In this work, the uniform oriented single crystalline anatase TiO_2 nano-pillar arrays were fabricated in tetramethylammonium hydroxide (TMAOH) solution by a simple hydrothermal method. Furthermore, we investigated the growth mechanism and photoelectrochemical properties of this TiO_2 nano-pillar arrays.

2. Experimental

The titanium plate (99.99% purity) with a size of 2.5 cm × 2.0 cm × 0.1 cm was polished, then washed by distilled

* Corresponding author. Tel.: +86 25 8489 5378; fax: +86 25 8489 5378.
E-mail address: taojie@nuaa.edu.cn (J. Tao).

0169-4332/$ – see front matter © 2009 Elsevier B.V. All rights reserved.
doi:10.1016/j.apsusc.2009.10.100

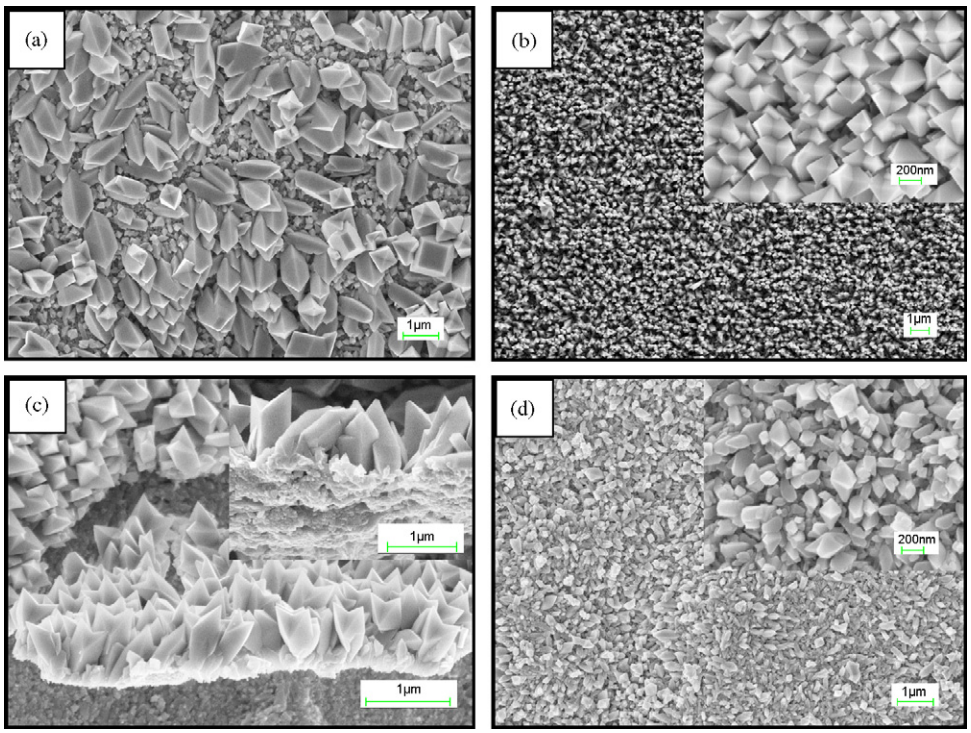

Fig. 1. FESEM images of vertically oriented TiO_2 nano-pillar arrays, (a), (b) and (d) images of the sample synthesized at 200 °C with 12 h, with the TMAOH concentration of 0.5 M, 1 M, 1.5 M, respectively. (c) Cross-sectional FESEM image of the TiO_2 nano-pillar arrays (TMAOH concentration is 1 M, inset shows the bottom parts of the nano-pillars arrays).

water, and dried in the oven. The sample was put into 60 ml solution of 1 M TMAOH in a 100 ml Teflon-lined stainless steel autoclave. The autoclave was heated to 160–220 °C for some hours in the oven. After the hydrothermal treatment, the specimen was completely washed with distilled water for several times. Finally, the sample was dried in the oven at 70 °C.

The morphologies of the samples were observed through field-emission scanning electron microscopy (FESEM) (LEO-1530VP) and transmission electron microscopy (TEM) (JEOL JEM-2100). The X-ray diffraction (XRD) measurement was performed with a Bruker D8 diffractometer with Cu Kα. Radiation operated at 40 kV, 36 mA (λ = 0.154056 nm). The Raman spectra were collected at

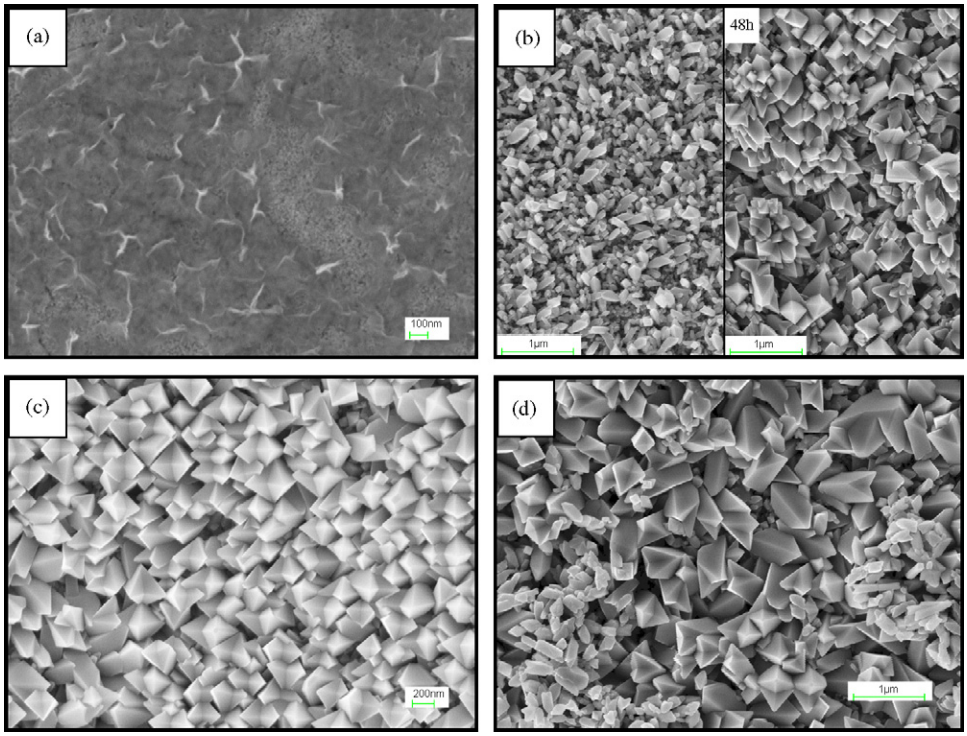

Fig. 2. FESEM images of different samples, (a), (b), (c) and (d) images of the sample synthesized at 160 °C, 180 °C, 200 °C, 220 °C for 12 h in 1 M TMAOH (the inset shows the image of sample synthesized at 180 °C, 48 h).

room temperature with a confocal Raman microscope (NT-MDT NTEGRA Spectra) using a 514 nm laser as the excitation source.

The photoelectrochemical properties of the as-prepared specimens were further investigated in three-electrode system with the aid of electrochemical workstation CHI (660B), using the Ti foil covered with the thin film of TiO_2 nano-pillar arrays, platinum electrode, saturated calomel electrode (SCE) as the working electrode, counter electrode, and reference electrode, respectively. The Hg lamp (~8 mW) was used for UV illumination. The sample size was 1.0 cm × 1.0 cm.

3. Results and discussion

Fig. 1 shows the FESEM images of as-prepared samples synthesized in different concentration of TMAOH solution at 200 °C for 12 h. In Fig. 1(b) and (c) the top-view and side-view images of nano-pillar arrays sample (prepared in 1 M TMAOH at 200 °C for 12 h, in short, S200-12-1), show that a high uniform TiO_2 nano-pillar arrays, with a size of 50–250 nm in width, 400–700 nm in length, and a tetrahydral bipyramidal tip are oriented in the vertical direction to the substrate. Fig. 1(c) shows cross-sectional view of S200-12-1, indicating that the TiO_2 nano-pillars are oriented in the vertical direction to the substrate. It is found that the bottom parts of the nano-pillars arrays (inset of Fig. 1(c)) are composed of a lot of small crystals, which may be destined for the nucleus of the nano-pillars arrays. When the Ti plate was treated in lower concentration of TMAOH solution (as shown in Fig. 1(a)), S200-12-0.5 (prepared in 0.5 M TMAOH at 200 °C for 12 h) is composed of two kinds of crystals. One is bigger tetrahydral bipyramidal nano-pillar (~700 nm in width, ~1500 nm in length) without uniform orientation, compared to S200-12-1, and the other is particulate crystal. Differently, when the sample is prepared in higher concentration of TMAOH solution (seen in Fig. 1(d)), the products S200-12-1.5 (prepared in 1.5 M TMAOH at 200 °C for 12 h) are just some un-oriented nanoparticles in irregular shape. Therefore, it can be concluded that the concentration of TMAOH is one of the key parameters for preparation of the tetrahydral bipyramidal nano-pillar arrays. According to these results, it is believed that the uniform tetrahydral bipyramidal nano-pillars can be synthesized only in 1 M TMAOH solution and the morphology of the products varies with the increase of the TMAOH concentration (from non-uniform tetrahydral bipyramidal nano-pillars to uniform tetrahydral bipyramidal nano-pillars, then to irregular nanoparticle).

The effect of the hydrothermal temperature on the product was also investigated by observing the samples synthesized at different temperatures (160, 180, 200, 220 °C) in 1 M TMAOH for 12 h, short for S160-12-1, S180-12-1, S200-12-1, and S220-12-1 respectively. As shown in Fig. 2, the uniform tetrahydral bipyramidal TiO_2 nano-pillar arrays were formed at 200 °C. There was nothing formed on the surface of the specimen prepared at 160 °C. When the hydrothermal temperature was increased to 180 °C, even prolonging hydrothermal time to 48 h (named S180-48-1), only some nano-crystals without a uniform morphology and orientation were observed (Fig. 2b). Based on FESEM observation of the sample S180-48-1 and S180-12-1, it can be observed that hydrothermal time just has an effect on the size of crystals (longer time induced larger size crystal), not on the orientation of the products. Fig. 2d presents the morphology of the samples synthesized at 220 °C. Obviously, tetrahydral bipyramidal nano-pillars were formed, accompanied with some irregular smaller crystals, but the orientation of the nano-pillars was random. The size of nano-pillar (S220-12-1) was about 200 nm in width, 700 nm in length, almost the same as that of S200-12-1. Accordingly, when the hydrothermal temperature is higher than 200 °C, the size of the nano-pillar almost keeps the same. Combining Fig. 1 and Fig. 2, it is revealed that the nano-pillar arrays could be formed in a suitable TMAOH concentration (1 M) and temperature (200 °C). According to the Oswald ripening mechanism, the crystal growth during the hydrothermal process is a dynamic equilibrium of dissolution and precipitation, which is affected by solution concentration, temperature, and other factors [19–21]. The same impacting effect was

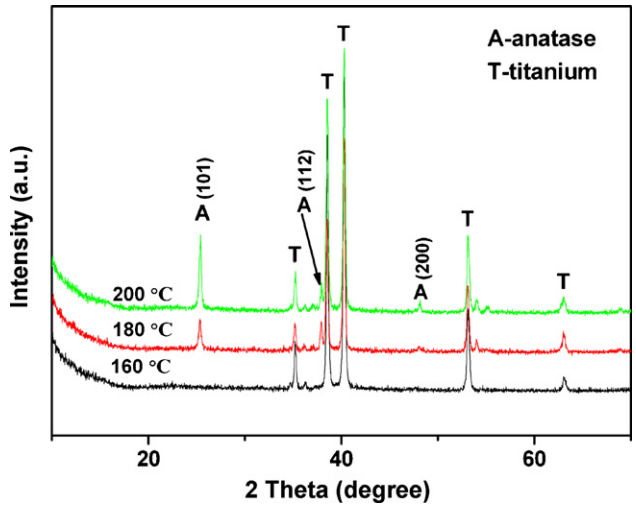

Fig. 3. XRD patterns of TiO_2 nano-pillars arrays samples synthesized in 1 M TMAOH, at different hydrothermal temperatures for 12 h.

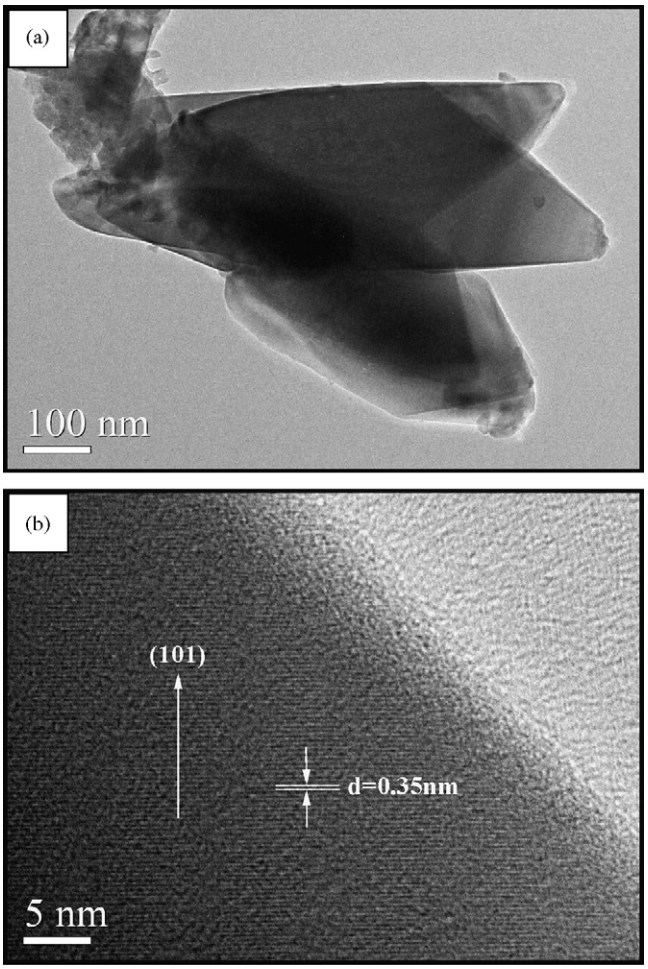

Fig. 4. TEM (a) and HRTEM (b) bright field images of TiO_2 nano-pillars prepared by hydrothermal crystallizing in 1 M TMAOH, at 200 °C for 12 h (sample S200-12-1).

determined in our research. The results clearly showed that the variation in solution concentration and hydrothermal temperature affects not only the morphology and size, but also the orientation of the products.

The XRD patterns of the samples (Fig. 3) demonstrate that the samples of S200-12-1 and S180-12-1 are constituted with anatase crystals. There are no characteristic peaks of TiO_2 (including brookite, anatase and rutile) in XRD pattern of S160-12-1, indicating that no TiO_2 formed, as the FESEM images also showed. Through comparing the XRD patterns of S200-12-1 and S180-12-1, it is found that the higher temperature induced higher intensity of the characteristic peaks of the anatase. In other words, the crystallinity of the products can be improved by increasing the hydrothermal temperature. Some reports have confirmed that TiO_2 with a high crystallinity is good for enhancing the efficiency of the DSSC [22,23]. Therefore, S200-12-1 with relatively higher crystallinity was chosen as anode of the DSSC. It is well known that the crystal form of the hydrothermal product can be changed through

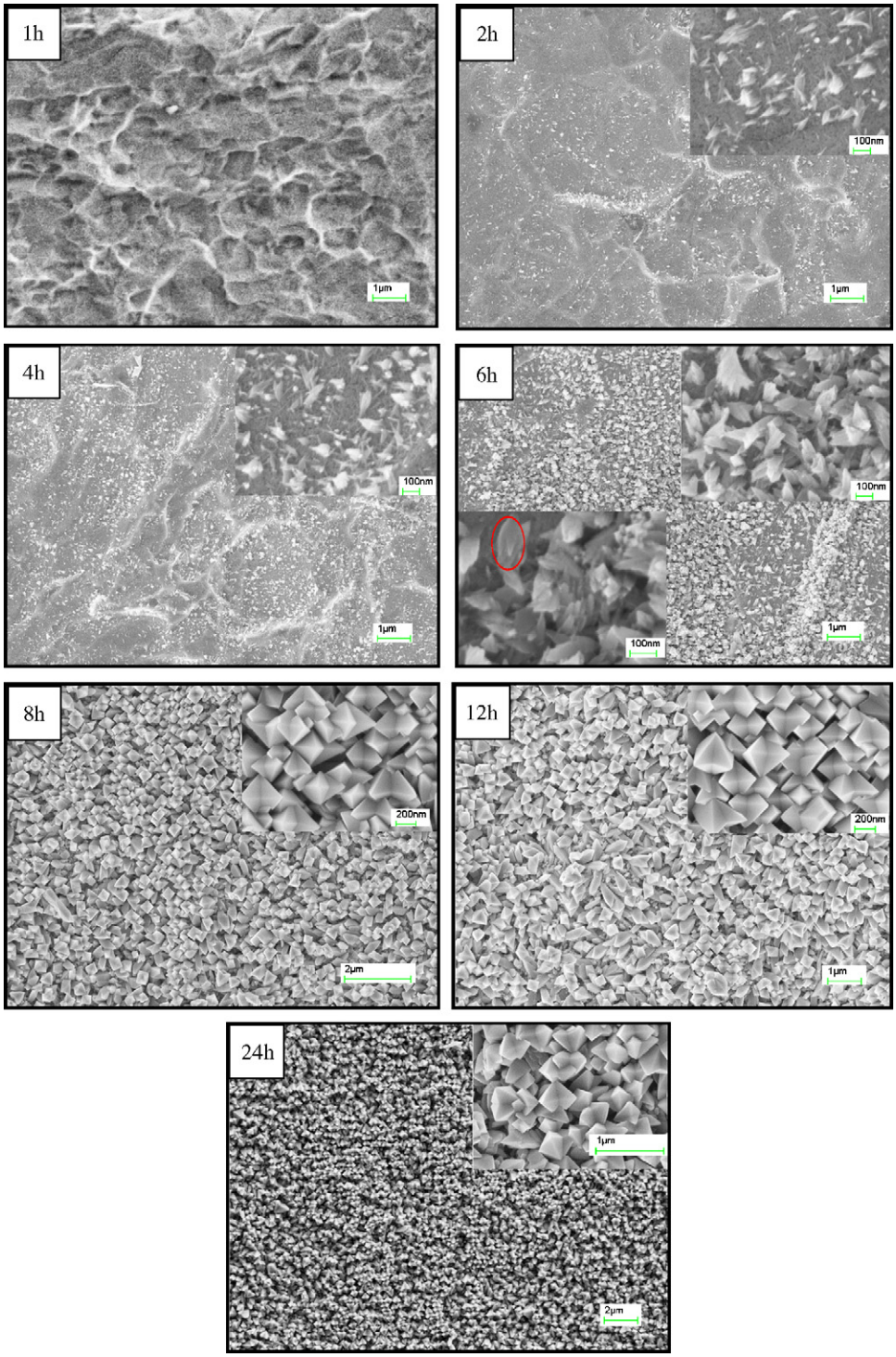

Fig. 5. FESEM images of the samples prepared by using 1 M TMAOH at 200 °C for different times: 1 h (S200-1-1), 2 h (S200-2-1), 4 h (S200-4-1), 6 h (S200-6-1), 8 h (S200-8-1), 12 h (S200-12-1), 24 h (S200-24-1).

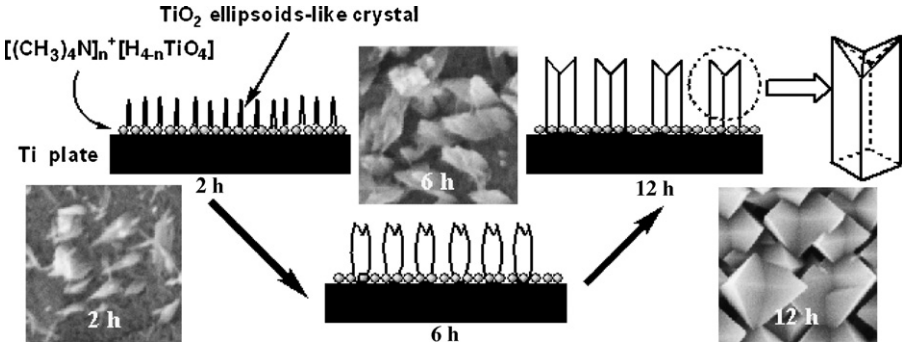

Fig. 6. Schematic growth of TiO_2 nano-pillar crystal.

adjusting the hydrothermal parameters, such as hydrothermal temperature, hydrothermal time, pH value and concentration of the solution.

TEM and HRTEM bright field images of the specimens are presented in Fig. 4. The nanorods are of a bipyramid rod-like shape with a size of ~250 nm in width, ~700 nm in length, in accord with the FESEM results. According to the calculations by Wu et al. [24–26], the TiO_2 nanocrystal with the bipyramid rod-like shape is more stable than the other shapes. The anatase (1 0 1) crystal faces can be observed in HRTEM image (Fig. 4(b)), which is consistent with the calculation by Oilver et al. [27]. The (1 0 1) crystal faces of anatase with lower surface energy are expected to be more stable than others.

While the concentration of TMAOH was kept at 1 M and the temperature was held at 200 °C, the growth process of the nano-pillar was observed to investigate its formation mechanism. The FESEM images of the samples synthesized for the different hydrothermal time are presented in Fig. 5. Before the hydrothermal process, the surface of the Ti substrate is relatively smooth. After 1 h of hydrothermal treatment (Fig. 5 (1 h)), the Ti substrate is chemically etched and the surface is rough. Few crystals are found during this period. When the sample was treated for 2 h (Fig. 5 (2 h)), a few of tiny TiO_2 crystals with rod shape appear on the Ti substrate. The formed TiO_2 nano-pillars grow larger and keep irregular shape when the hydrothermal time is increased to 4 h (Fig. 5 (4 h)). A large number of TiO_2 nano-pillars with a bigger size can be obtained after 6 h hydrothermal treatment, compared with the sample (4 h treatment), as shown in Fig. 5 (6 h). It is easily found that the nano-pillars with a tetrahydral bipyramidal tip are formed (as the circle marked). And the tetrahydral bipyramidal nano-pillars arrays are gained after 8 h hydrothermal treatment (seen in Fig. 5 (8 h)). The size of the nano-pillar is almost maintained even after increasing the hydrothermal time to 12 h and 24 h (Fig. 5 (12 h) and Fig. 5 (24 h)).

TMAOH as a kind of organic alkali will react with Ti to form tetramethylammonium titanate ($[(CH_3)_4N]_n^+[H_{4-n}TiO_4]$, $n = 1–4$) with a layered structure, and titanate layers interact with each other through hydrogen bonds [28,29]. It is presumed that TMAOH does not react completely with Ti (the final pH value >7), then, free tetramethylammonium cation (TMA^+) and OH^- are still in the solution. The isoelectric point of TiO_2 is about 6.0–6.7, and TiO_2 is of negative charge in alkaline conditions. Therefore, TMA^+ is trapped or constrained by layered tetramethylammonium titanate. Then, TMAOH is degraded into neutral trimethylamine (TMA) molecule not TMA^+ with positive charge under the high hydrothermal temperature (200 °C). As a result of the hydrothermal treatment, the layered structure of tetramethylammonium titanate is destroyed. In addition, TMA can selectively adsorb on the lattice planes parallel to (0 0 1) of anatase TiO_2 through hydrogen bonding. Some reports have also confirmed that TMA units can be bonded on the facets whose normal direction is [1 0 0] [28,30]. On the other hand, amine groups also have a specific affinity to the planes parallel to the *c*-axis of the tetragonal system, leading to an ellipsoids-like shape of the particle [30]. Therefore, when the Ti plate is autoclaved at 200 °C, the growth rate of the crystal planes of anatase TiO_2 parallel to *c*-axis is limited [28]. The crystals grow along *c*-axis with the hydrothermal time prolonging (as shown in Fig. 5). Simultaneously, the TMAOH as a structure template can make the single-phase anatase to be arranged regularly during the hydrothermal process. The same conclusions have been reported in the former works [28,31,32]. Fig. 6 well presents the crystal growth process. The crystal growth process includes: the reaction of TMAOH and Ti, the diffusion of the layered tetramethylammonium titanate and the crystallization of tetramethylammonium titanate. First, TMAOH reacts with Ti to form the layered tetramethylammonium titanates, as Fig. 6 shows. Then, the layered structure of tetramethylammonium titanates is destroyed as a result of the hydrothermal treatment. The tetramethylammonium titanates with destroyed layered structure diffuse to the solution, providing the Ti source for TiO_2 crystals. At last, the ellipsoids-like TiO_2 crystals grow on the surface of Ti plate with the aid of the selectively absorptions of TMA units and amine groups under hydrothermal condition, as seen in Fig. 6. The continuous repetition of these steps induces the final TiO_2 nano-pillar arrays. Certainly, further study is needed to explore the detailed mechanism of the configured structure and the effects of other ions on the crystal growth.

Raman spectroscopy is a very useful tool to characterize various crystalline phases of titania thin film [33–35]. Fig. 7 shows the Raman spectrum of S200-12-1. It can be seen six Raman peaks at

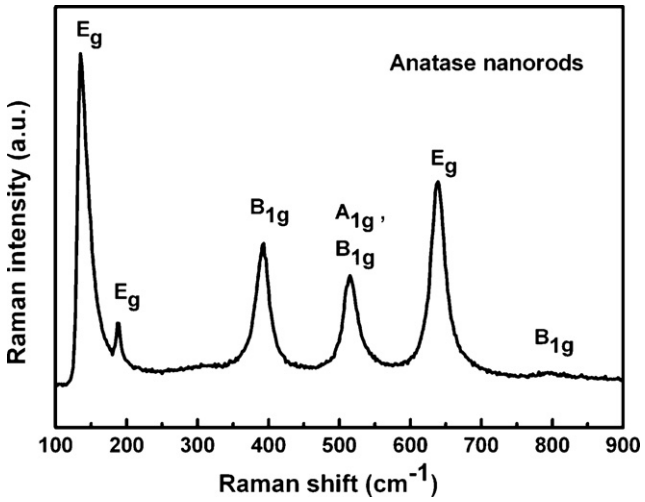

Fig. 7. Raman spectra of sample S200-12-1 (synthesized in 1 M TMAOH, at 200 °C for 12 h).

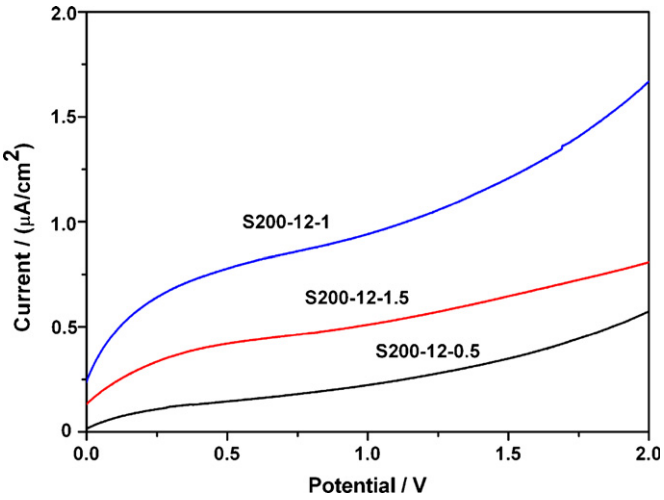

Fig. 8. Variation of photocurrent density *vs* applied electrode potential for S200-12-0.5, S200-12-1, and S200-12-1.5 in 0.5 M Na_2SO_4 under Hg lamp (~8 mW) irradiation.

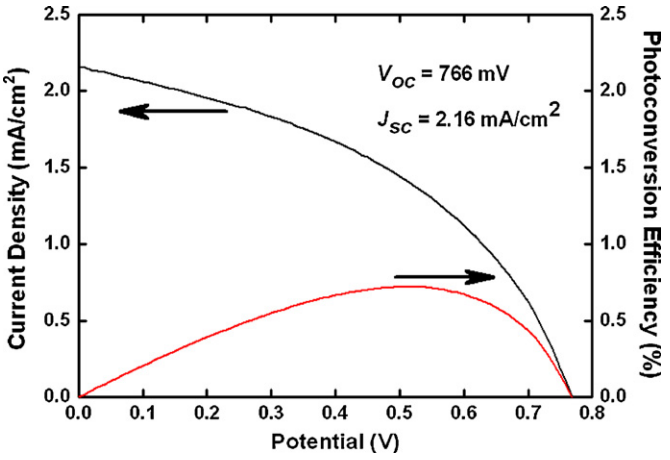

Fig. 10. Photocurrent density (black), and power density (red) of 700 nm long TiO_2 nano-pillar arrays based dye-sensitized solar cells under AM 1.5 illumination (100 mW/cm^2). (For interpretation of the references to color in this figure legend, the reader is referred to the web version of the article.)

135, 188, 392, 515, 638, 792 cm^{-1} in Fig. 7 were assigned to E_g, E_g, B_{1g}, A_{1g} (including B_{1g}), E_g, and B_{1g}, respectively. The peak at 515 cm^{-1} should be superposition of two modes (A_{1g} and B_{1g}), because the band at 515 cm^{-1} would be resolved into two components at 507 cm^{-1} (A_{1g}) and 519 cm^{-1} (B_{1g}) only below 73 K [35]. In comparison with Ref. [36], the positions of the six Raman active modes are a little deviated. This deviation may be caused by some impurities. Therefore, just pure anatase TiO_2 peaks can be observed in the Raman spectrum of S200-12-1.

Furthermore, the photoelectrochemical properties of the samples were studied by means of linear sweep voltammetry. Fig. 8 is the typical photocurrent density *vs* applied potential curves of the specimens prepared in different concentration of TMAOH at 200 °C for 12 h in 0.5 M Na_2SO_4 supporting electrolyte under UV (~8 mW Hg lamp) illumination. Under UV illumination, the photoelectrochemical response appeared for all three thin films. The photocurrents density increased in the order of S200-12-1 > S200-12-1.5 > S200-12-0.5. S200-12-1 composed of the uniform nano-pillar arrays exhibited the largest photocurrent density, as a result of the few grain boundaries and direct electron transferring pathway of the pure anatase TiO_2 nano-pillar [20,21,37].

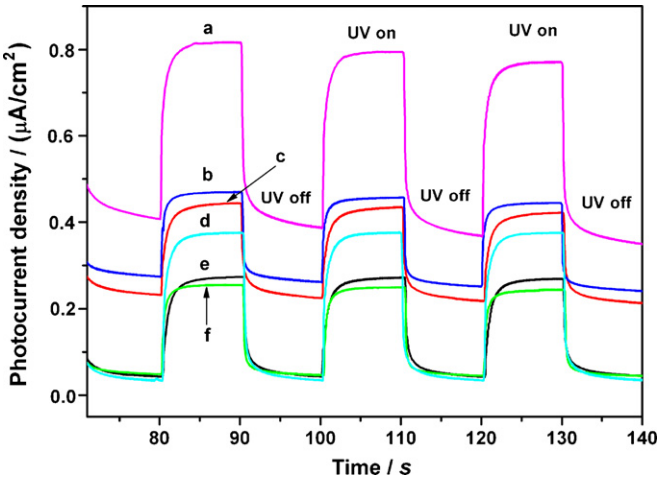

Fig. 9. Photocurrent response curves of the S200-12-1 (a and d, at 1.5, 0.5 V, respectively), S200-12-1.5 (b and e, at 1.5, 0.5 V, respectively), S200-12-0.5 (c and f, at 1.5, 0.5 V, respectively) at different applied electrode potential in 0.5 M Na_2SO_4 under Hg lamp (~8 mW) pulsed-irradiation.

Photocurrent transient measurement method was also adopted to examine the photoelectrochemical properties of these three kinds of thin films (as Fig. 9 shown). The steady-state photocurrent density of S200-12-1 was about 1.5 times as large as that of S200-12-1.5 or S200-12-0.5 (photocurrent densities of the S200-12-1, S200-12-1.5, S200-12-0.5 films in Fig. 9 are 0.816, 0.469, 0.442 μA/cm^2, at the 1.5 V applied bias potential, respectively). It can be seen that the photocurrents of all specimens keep at a constant value in the dark. When the UV light is on, the photocurrents increase rapidly, and then gradually rise to a steady state. When the UV light is off, the photocurrents fall back to previous value (in the dark) in a few seconds. Simultaneously, the photocurrent is in direct proportion to the applied potential (photocurrent densities of the S200-12-1 are 0.375, 0.816 μA/cm^2, at 0.5 V and 1.5 V applied bias potential, respectively), showing the same changing trend of Fig. 8. The relatively higher photocurrent response of S200-12-1 can be explained in terms of high activity of the single crystal anatase TiO_2 and direct electrical pathway for photogenerated electrons and enhanced the electron transport rate induced by the uniform orientation of the TiO_2 nano-pillar arrays.

The preliminary DSSC was assembled using typical TiO_2 nano-pillar arrays film with 700 nm thickness as the photo-anode according to the fabrication method described previously [6,7]. Fig. 10 shows the current–voltage characteristic of typical DSSC. An overall conversion efficiency of 0.72% is achieved, with an open circuit voltage (V_{oc}) of 0.766 V and short circuit current density (J_{sc}) of 2.16 mA cm^{-2}. Efficient vectorial charge transport (as Figs. 8 and 9 show) ability of the single crystal anatase nano-pillar arrays make us believe that significantly higher efficiencies can reasonably be expected through optimizing sizes of the TiO_2 arrays and fabrication technology.

4. Conclusions

(1) Using a new chemical route based on hydrothermal method, the oriented single crystalline titanium dioxide (TiO_2) nano-pillar arrays were successfully prepared on the surface of Ti plate. Ti plate provides not only the substrate for TiO_2 arrays but also the Ti source of TiO_2. The TiO_2 nano-pillar was pure anatase with a tetrahydral bipyramidal tip.

(2) Both TMAOH concentration and the hydrothermal temperature determined the uniformity and orientation of TiO_2 nano-pillar

arrays. The uniform orientated TiO_2 nano-pillar arrays could be prepared in 1 M TMAOH, at 200 °C for more than 8 h.

(3) The uniformly orientated TiO_2 nano-pillar arrays thin film presented superior photoelectrochemical properties in 0.5 M Na_2SO_4, which is ascribed to less grain boundaries and direct electrical pathway for electron transferring. We are sure that these uniform orientated TiO_2 nano-pillar arrays are a promising candidate for DSSC, owing to the outstanding photoelectrodchemical characteristics. Certainly, the sizes of the TiO_2 nano-pillar arrays and fabrication technology should be optimized to enhance the efficiency of the DSSC based on this kind of TiO_2 nano-pillar arrays.

References

[1] N. Negishi, T. Iyoda, K. Hashimoto, A. Fujishima, Preparation of transparent TiO_2 thin-film photocatalyst and its photocatalytic activity, Chem. Lett. 9 (1995) 841–842.

[2] S. Colodrero, M. Ocana, H. Miguez, Nanoparticle-based one-dimensional photonic crystals, Langmuir 24 (2008) 4430–4434.

[3] U. Bach, D. Lupo, P. Comte, J.E. Moser, F. Weissortel, J. Salbeck, H. Spreitzer, M. Gratzel, Solid-state dye-sensitized mesoporous TiO_2 solar cells with high photon-to-electron conversion efficiencies, Nature 395 (1998) 583–585.

[4] X. Wang, C. Neff, E. Graugnard, Y. Ding, J.S. King, L.A. Pranger, R. Tannenbaum, Z.L. Wang, C.J. Summers, Photonic crystals fabricated using patterned nanorod arrays, Adv. Mater. 17 (2005) 2103–2106.

[5] X.B. Chen, S.S. Mao, Titanium dioxide nanomaterials: synthesis, properties, modifications, and applications, Chem. Rev. 107 (2007) 2891–2959.

[6] B. Liu, E.S. Aydil, Growth of oriented single-crystalline rutile TiO_2 nanorods on transparent conducting substrates for dye-sensitized solar cells, J. Am. Chem. Soc. 131 (2009) 3985–3990.

[7] X.J. Feng, K. Shankar, O.K. Varghese, M. Paulose, T.J. Latempa, C.A. Grimes, Vertically aligned single crystal TiO_2 nanowire arrays grown directly on transparent conducting oxide coated glass: synthesis details and applications, Nano Lett. 8 (2008) 3781–3786.

[8] X. Peng, A. Chen, Dense and high-hydrophobic rutile TiO_2 nanorod arrays, Appl. Phys. A Mater. 80 (2005) 473–476.

[9] G. Centi, R. Passalacqua, S. Perathoner, D.S. Su, G. Weinberg, R. Schlogl, Oxide thin films based on ordered arrays of 1D nanostructure. A possible approach toward bridging material gap in catalysis, Phys. Chem. Chem. Phys. 9 (2007) 4930–4938.

[10] Y. Liu, W. Chen, Y. Yang, J.L. Ong, K. Tsuru, S. Hayakawa, A. Osaka, Novel fabrication of nano-rod array structures on titanium and in vitro cell responses, J. Mater. Sci: Mater. Med. 19 (2008) 2735–2741.

[11] Q. Wei, K. Hirata, K. Tajima, K. Hashimoto, Design and synthesis of TiO_2 nanorod assemblies and their application for photovoltaic devices, Chem. Mater. 18 (2006) 5080–5087.

[12] W. Smith, Y. Zhao, Enhanced photocatalytic activity by aligned WO_3/TiO_2 two-layer nanorod arrays, J. Phys. Chem. C 112 (2008) 19635–19641.

[13] C.A. Chen, K.Y. Chen, Y.S. Huang, D.S. Tsai, K.K. Tiong, F.Z. Chien, X-ray diffraction and Raman scattering study of thermal-induced phase transformation in vertically aligned TiO_2 nanocrystals grown on sapphire(1 0 0) via metal organic vapor deposition, J. Cryst. Growth 310 (2008) 3663–3667.

[14] X. Dong, J. Tao, Y.Y. Li, H. Zhu, Enhanced photoelectrochemical properties of F-containing TiO_2 sphere thin film induced by its novel hierarchical structure, Appl. Surf. Sci. 255 (2009) 7183–7187.

[15] J. Wu, Low-temperature preparation of titania nanorods through direct oxidation of titanium with hydrogen peroxide, J. Cryst. Growth 269 (2004) 347–355.

[16] J. Wu, T. Zhang, Y. Zeng, S. Hayakawa, T. Kanji, A. Osaka, Large-scale preparation of ordered titania nanorods with enhanced photocatalytic activity, Langmuir 21 (2005) 6995–7002.

[17] Z.R. Tian, J.A. Voigt, J. Liu, B. Mckenzie, H. Xu, Large oriented arrays and continuous films of TiO_2-based nanotubes, J. Am. Chem. Soc. 125 (2003) 12384–12385.

[18] C.C. Wang, J.Y. Ying, Sol-gel synthesis and hydrothermal processing of anatase and rutile titania nanocrystals, Chem. Mater. 11 (1999) 3113–3120.

[19] P.D. Cozzoli, A. Kornowski, H. Weller, Low-temperature synthesis of soluble and processable organic-capped anatase TiO_2 nanorods, J. Am. Chem. Soc. 125 (2003) 14539–14548.

[20] H.G. Yang, H.C. Zeng, Preparation of hollow anatase TiO_2 nanospheres via Ostwald ripening, J. Phys. Chem. B 108 (2004) 3492–3495.

[21] A. Zaban, S.T. Aruna, S. Tirosh, B.A. Gregg, Y. Mastai, The effect of the preparation condition of TiO_2 colloids on their surface structures, J. Phys. Chem. B 104 (2000) 4130–4133.

[22] M.S. Akhtar, M.A. Khan, M.S. Jeon, O. Yang, Controlled synthesis of various ZnO nanostructured materials by capping agents-assisted hydrotherm method for dye-sensitized solar cells, Electrochim. Acta 53 (2008) 7869–7874.

[23] K. Hou, B. Tian, F. Li, Z. Bian, D. Zhao, C. Huang, Highly crystallized mesoporous TiO_2 films and their applications in dye sensitized solar cells, J. Mater. Chem. 15 (2005) 2414–2420.

[24] J. Wu, S. Hao, J. Lin, M. Huang, Y. Huang, Z. Lan, P. Li, Crystal morphology of anatase titania nanocrystals used in dye-sensitized solar cells, Cryst. Growth Des. 8 (2008) 247–252.

[25] R.L. Penn, J.F. Banfield, Morphology development and crystal growth in nanocrystalline aggregates under hydrothermal conditions: insights from titania, Geochem. Cosmochim. Acta 63 (1999) 1549–1557.

[26] H. Zhang, J.F. Banfield, Thermodynamic analysis of phase stability of nanocrystalline titania, J. Mater. Chem. 8 (1998) 2073–2076.

[27] P.M. Oliver, G.W. Watson, E.T. Kelsey, S.C. Parker, Atomistic simulation of the surface structure of the TiO_2 polymorphs rutile and anatase, J. Mater. Chem. 7 (1997) 563–568.

[28] Y. Chen, X. He, X. Zhao, Q. Yuan, X. Gu, Preparation, characterization, and growth mechanism of a novel aligned nanosquare anatase in large quantities in the presence of TMAOH, J. Colloid Interface Sci. 310 (2007) 171–177.

[29] C. Liu, A. Rouet, H. Sutrisno, E. Puzenat, H. Terrisse, L. Brohan, M. Richard-Plouet, Low temperature synthesis of nanocrystallized titanium oxides with layered or tridimensional frameworks, from $[Ti_8O_{12}(H_2O)_{24}]Cl_8{\cdot}HCl_7{\cdot}H_2O$ hydrolysis, Chem. Mater. 20 (2008) 4739–4748.

[30] T. Sugimoto, X. Zhou, A. Muramatsu, Synthesis of uniform anatase TiO_2 nanoparticles by gel–sol method: 4. Shape control, J. Colloid Interface Sci. 259 (2003) 53–61.

[31] V. Shklover, M.K. Nazeeruddin, S.M. Zakeeruddin, C. Barbe, A. Kay, T. Halbach, W. Steurer, R. Hermann, H.U. Nissen, M. Gratzel, Structure of nanocrystalline TiO_2 powders and precursor to their highly efficient photosensitizer, Chem. Mater. 9 (1997) 430–439.

[32] S.D. Burnside, V. Shklover, C. Barbe, P. Comte, F. Arendse, K. Brooks, M. Gratzel, Self-organization of TiO_2 nanoparticles in thin films, Chem. Mater. 10 (1998) 2419–2425.

[33] S.W. Lu, C. Harris, S. Walck, M. Arabab, Phase sensitivity of Raman spectroscopy analysis of CVD titania thin films, J. Mater. Sci. 44 (2009) 541–544.

[34] L.J. Hardwich, M. Holzapfel, P. Novak, L. Dupont, E. Baudrin, Electrochemical lithium insertion into anatase-type TiO_2: an in situ Raman microscopy investigation, Electrochim. Acta 52 (2007) 5357–5367.

[35] T. Ohsaka, F. Izumi, Y. Fujiki, Raman spectrum of anatase, TiO_2, J. Raman Spectrosc. 7 (1978) 321–324.

[36] L. Miao, S. Tanemura, S. Toh, K. Kaneko, M. Tanemura, Fabrication, characterization and Raman study of anatase-TiO_2 nanorods by a heating-sol–gel template process, J. Cryst. Growth 264 (2004) 246–252.

[37] W. Wang, H. Lin, J. Li, N. Wang, Formation of titania nanoarrays by hydrothermal reaction and their application in photovoltaic cells, J. Am. Ceram. Soc. 91 (2008) 628–631.